Crystal Structures and Magnetic Properties of the New Alkaline Zinc Oxovanadium Phosphates $MZn(H_2O)(VO)_2(PO_4)_2(H_2PO_4)$ with $M = K^+$, Rb^+, and Cs^+

S. Messaoudi,† E. Furet,† R. Gautier,† E. Le Fur,† O. Peña,‡ and J. Y. Pivan*,†

Laboratoire de Physicochimie, UPRES 1795, Ecole Nationale Supérieure de Chimie de Rennes, and Laboratoire de Chimie du Solide et Inorganique Moléculaire, UMR 6511 CNRS-Université de Rennes 1, Institut de Chimie de Rennes, Campus de Beaulieu, Avenue du Général Leclerc, 35700 Rennes, France

Received June 5, 2003. Revised Manuscript Received September 25, 2003

New alkaline oxovanadium phosphates of composition $MZn(H_2O)(VO)_2(PO_4)_2(H_2PO_4)$ (hereafter noted as MZnVPO's) were prepared hydrothermally for $M^+ = K^+$, Rb^+, Cs^+ that crystallize in the monoclinic symmetry. The compounds CsZnVPO and KZnVPO are isotypic (space group $P2_1/m$), whereas RbZnVPO shows a supercell (space group $P2_1/n$). All the three structures are based on linking of fused octahedra V_2O_9 with tetrahedra H_xPO_4 and $ZnO_3(H_2O)$ with the counterbalancing alkaline ions located inside the voids of the three-dimensional framework $[Zn(H_2O)(VO)_2(PO_4)_2(H_2PO_4)]^-$. Thermal analyses coupled with IR measurements support the structural results, and low-dimensional magnetism showing strong antiferromagnetic interactions is discussed.

Introduction

Much attention is devoted to the vanadium phosphorus oxides (hereafter noted as MVPO's) aiming at the synthesis of new catalysts, and the discovery of numerous solids with more or less intricate frameworks has resulted.[1] Additionally, these phases have been a field of intense theoretical research over the past decade as they frequently provide low dimensional quantum spin systems.[2−4] Hydrothermal conditions offer one of the most convenient routes to obtain such solids. The different mechanisms involved during the syntheses under hydrothermal conditions are not clearly understood, nevertheless kinetic effects are seemingly very important. We used for a long time a synthetic route with metallic zinc as reducing agent, and the solids obtained were either MZnVPO's (long reaction time) or MVPO's (short reaction time). Our results showed that the MZnVPO's can be thought as MVPO's with the Zn^{2+} centers playing the role of "reticulating" agents insofar as the same structural building units (SBU) are present in the structures.[5−7]

In this context, we report herein on the structures and thermal and magnetic behaviors of the new alkaline oxovanadium phosphates $MZn(H_2O)(VO)_2(PO_4)_2(H_2PO_4)$ with $M^+ = K^+$, Rb^+, and Cs^+ containing dimers V_2O_9.

Experimental Section

Synthesis. Mixtures of vanadium pentoxide, M_2CO_3, and metallic zinc were heated in hydrothermal conditions in the presence of 85% orthophosphoric acid and water. Typically, the reactants were introduced in the ratio V_2O_5 (∼0.8 mmol), M_2CO_3 (∼1.5 mmol), Zn^0 (∼3 mmol), and added to 5 mL of a solution of ∼2 M H_3PO_4. The initial mixtures were sealed in a 23-mL Teflon lined acid digestion bomb (Parr Instruments), then heated at 245 °C under autogenous pressure for 6 days. After slowly cooling to room temperature, the reaction products were filtered off, washed with distilled water, and dried in air in a furnace maintained at 100 °C for 24 h. Visual examination under the microscope revealed the bulk products to be polyphasic, especially for the cesium and rubidium preparations. Tentatives in obtaining samples free of impurities were successful for KZnVPO and RbZnVPO that were recovered as blue powders. A degassed sample of KZnVPO was immersed at room temperature in CH_2Cl_2 (Archimede's principle) and density $\rho = 2.88$ g·cm^{-3} was obtained. Whatever the conditions used, the CsZnVPO compound has been obtained as minor components. Blue platelet well-shaped single crystals suitable for structure determination were isolated for all three compounds.

X-ray Diffraction Studies. X-ray powder diffraction patterns were recorded using Cu Kα radiation ($\lambda = 1.54178$ Å) for KZnVPO and RbZnVPO. All the diffraction peaks of the X-ray patterns were indexed using DICVOL91[8] on the basis of a monoclinic unit cell. The parameters obtained and the corresponding figures of merit are $a = 9.317(1)$ Å, $b = 9.212(2)$ Å, $c = 7.445(1)$ Å, $\beta = 104.29(2)°$, $M_{30}/F_{30} = 23.3/41.8(0.0085, 84)$ for KZnVPO, and $a = 9.471(3)$ Å, $b = 9.232(5)$ Å, $c = 7.502(5)$ Å, $\beta = 101.21(6)°$ $M_{20}/F_{20} = 16.7/21.4(0.0146, 64)$ for RbZnVPO.

Single-crystal diffraction experiments were conducted at room temperature using an Enraf-Nonius diffractometer with

* To whom correspondence should be addressed. Fax: + 2 23 23 81 99. E-mail: jean-yves.pivan@ensc-rennes.fr.
† Laboratoire de Physicochimie.
‡ Laboratoire de Chimie du Solide et Inorganique Moléculaire.

(1) Boudin, S.; Guesdon, A.; Leclaire, A.; Borel, M.-.M. *Int. J. Inorg. Mater*. **2000**, *2*, 561, and references therein.
(2) Johnston, D. C.; Johnson, J. W.; Goshorn, D. P.; Jacobson, A. J. *Phys. Rev. B* **1987**, *35*, 219.
(3) Barnes, T.; Riera, J. *Phys. Rev. B* **1994**, *50*, 6817.
(4) Prokofiev, A. V.; Büllesfeld, F.; Assmus, W.; Schwenk, H.; Wichert, D.; Löw, U.; Lüthi, B. *Eur. Phys. J. B* **1998**, *5*, 313.
(5) Le Fur, E.; Moreno, Y.; Pivan, J.-Y. *J. Mater. Chem*. **2001**, *11*, 1735.
(6) Le Fur, E.; Peña, O.; Pivan, J.-Y. *J. Mater. Chem*. **2002**, *12*, 132.
(7) Le Fur, E.; Pivan, J.-Y. *Solid State Sci.* **2002**, *4*, 233.
(8) Louër, D.; Boultif, M. *J. Appl. Crystallogr*. **1991**, *24*, 987.

10.1021/cm031090k CCC: $27.50
Published on Web 12/25/2003

Table 1. Crystal Data and Summary of Data Collection, Structure Solution, and Refinement for $KZn(H_2O)(VO)_2(PO_4)_2(H_2PO_4)$ (1) , $CsZn(H_2O)(VO)_2(PO_4)_2(H_2PO_4)$ (2), and $RbZn(H_2O)(VO)_2(PO_4)_2(H_2PO_4)$ (3)

crystal data	(**1**)	(**2**)	(**3**)
color; habit		blue; plates	
crystal system		monoclinic	
space group	$P2_1/m$ (n°11)	$P2_1/m$ (n°11)	$P2_1/n$
Unit cell dimensions	$a = 7.4459(1)$ Å	$a = 7.5159(1)$ Å	$a = 10.8586(2)$ Å
	$b = 9.2160(2)$ Å	$b = 9.1994(1)$ Å	$b = 9.1973(2)$ Å
	$c = 9.3199(2)$ Å	$c = 9.5465(2)$ Å	$c = 13.1673(3)$ Å
	$\beta = 104.281(1)°$	$\beta = 99.912(1)°$	$\beta = 103.501(1)°$
volume (Å^3)	619.78(2) Å^3	650.22(2) Å^3	1278.67(5)
Z		4	
formula weight	543.29 g·mol^{-1}	637.09 g·mol^{-1}	589.66 g·mol^{-1}
density (calc.)	2.911 g·cm^{-3}	3.254 g·cm^{-3}	3.063 g·cm^{-3}
absorption coefficient	42.1 cm^{-1}	65.5 cm^{-1}	75.3 cm^{-1}
maximum 2θ collected	$2\theta \leq 74°$	$2\theta \leq 70°$	$2\theta \leq 74°$
data in refinement	h: −12, +12	h: −12, +12	h: −18, +18
	k: −15, +15	k: −12, +14	k: −14, +15
	l: −15, +15	l: −15, +15	l: −22, +22
unique data after merging	3318	2998	6522
observed data ($> 2\sigma(F_o^2)$)	2639	2620	4636
free parameters	134	131	237
$R_{int.}$	0.032	0.044	0.039
residuals R ($> 2\sigma(F_o^2)$)	0.047	0.049	0.047
wR	0.092	0.108	0.092
extinction coefficient	0.022(2)	0.051(3)	0.0058(3)
min., max. (e/Å^3)	−1.21, +1.87	−1.52, +1.62	−2.16, +2.26
GOF	2.10	2.48	1.66

graphite monochromated Mo Kα radiation ($\lambda = 0.71073$ Å) and equipped with a CCD detector. The intensity data collection was performed in the ω-ϕ scanning mode with the goniometer and detector angular settings optimized using the program COLLECT.[9] The crystal-to-detector distance was 25 mm. The unit cell and the orientation matrix were refined using the entire data set of reflections. The diffraction spots were measured in full with a high accuracy, scaled with SCALEPACK, corrected for Lorentz-polarization correction, and integrated using DENZO.[9] The crystallographic data and conditions for structure analysis are listed in Table 1. Structure solutions (SIR97)[10] and refinements (SHELXL-97)[11] were run in the space groups $P2_1/m$ (KZnVPO and CsZnVPO) and $P2_1/n$ (RbZnVPO). The structure model (non-hydrogen atoms) was readily obtained from successive difference Fourier maps. At the end of refinement, anisotropic displacement parameters and extinction coefficients were allowed to vary, and the residuals listed in Table 1 resulted.

Infrared Spectroscopy. Samples of KZnVPO were pelletized in dry KBr and the measurements were run at room temperature using a Shimadzu FTIR 8300.

Chemical Analyses. Quantitative composition analyses (EPMA) were performed either on a JEOL JSM-6400 by energy-dispersive spectroscopy (EDS) of X-rays or on a Camebax SX-50 using wavelength-dispersive spectroscopy (WDS) of X-rays (GaP, V, Zn, ZnS, orthose (K 13.03%, Na 0.33%, Al 9.09%, Fe 0.88%, Si 30.56%, O 46.11%), vanadinite (Cl 2.62%, V 10.48%, Pb 73.8%, O 13.1%), and apatite (Ca 39.02%, Cl 0.35%, F 3.40%, P 18.32%, O 38.91%) as standards). The oxygen and hydrogen content of the phases was not determined because the water readily evaporates from local heating of the samples by the electron beam during analysis. EPMA measurements were found to be in good agreement with the phase compositions obtained from single-crystal data refinements (vide infra).

Thermogravimetric Measurements. Thermogravimetric analyses were performed using a Shimadzu thermogravimetric analyzer on samples of KZnVPO and RbZnVPO up to 900 K in flowing N_2 with a rate of 5 K/min. For both compounds, a two-step mechanism occurs upon heating: the weight decreases smoothly from 500 K then increases abruptly at about 750 K (Figure 1). The overall loss of weight (6.4% and 5.9% for KZnVPO and RbZnVPO, respectively) is attributed to dehydration processes (vide infra). The resulting products were amorphous and were not identified.

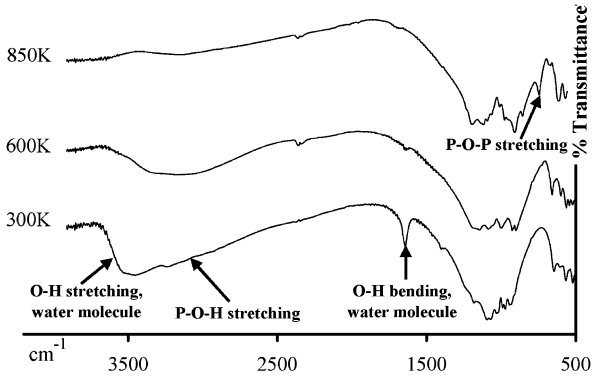

Figure 1. IR spectra of KZnVPO showing that the water molecule in the near neighboring of the zinc atoms is removed prior to the formation of condensed phosphate species.

Magnetic Susceptibility Studies. The susceptibility measurements were made on 256.2 mg (KZnVPO) and 282.4 mg (RbZnVPO) of zero-field-cooled powder samples. The experiments were carried out at 0.5 T (KZnVPO) and 0.1 T (RbZnVPO) in the temperature range 5−300 K with a SQUID (SHE) magnetometer-susceptometer. With decreasing temperature, the susceptibility first reaches smoothly a broad maximum at $T \approx 50$ K, decreases rapidly to a minimum at $T \approx 12$ K, then increases as the temperature is lowered. From the χT curve, antiferromagnetic interactions are the prevailing ones with respect to the negative deviation observed as the temperature decreases. The high-temperature part of the reciprocal susceptibility is well-described by a Curie−Weiss law $\chi = C/(T - \theta)$ with $\theta \approx -30$ K and an effective moment per V^{4+} ion $\mu_{exp} \approx 1.70\ \mu_B$ that compares well with the value 1.73 μ_B for an $S = 1/2$ ion.

Structure Results

Linking of V_2O_9 dimers with $ZnO_3(H_2O)$, PO_4, and H_2PO_4 tetrahedra leads to the formation of the three-

(9) COLLECT, DENZO, SCALEPACK, SORTAV, Kappa CCD Program Package; Nonius BV: Delft, The Netherlands, 1998.

(10) Altomare, A.; Burla, M. C.; Camalli, M.; Cascarano, G. L.; Giacovazzo, C.; Guagliardi, A.; Moliterni, A. G. G.; Polidori, G.; Spagna, R. *J. Appl. Crystallogr.* **1999**, *32*, 115.

(11) Sheldrick. G. M. *SHELXL-97, Program for crystal structure refinement*: University of Göttingen: Germany, 1997.

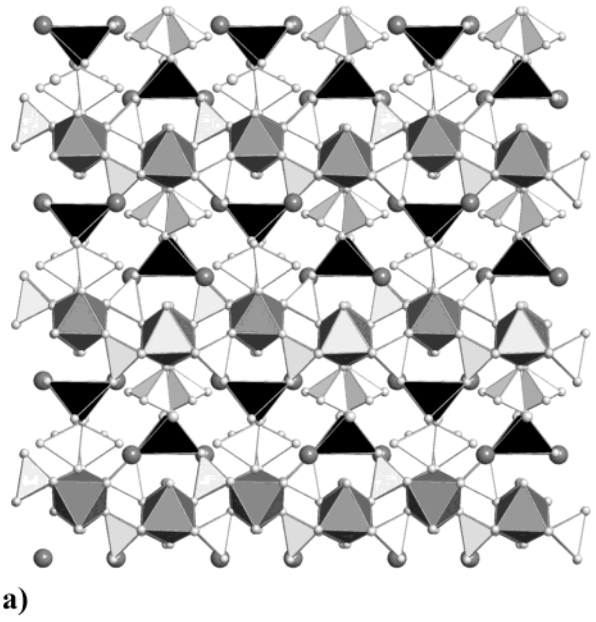

Figure 2. View of $CsZn(H_2O)(VO)_2(PO_4)_2(H_2PO_4)$ along the [100] direction (a) and the [001] direction (b): dark gray polyhedra, VO_6; light gray, PO_4 and H_2PO_4; black, $Zn(H_2O)O_3$.

dimensional structure of $MZn(H_2O)(VO)_2(PO_4)_2(H_2PO_4)$. The structure is shown in Figure 2. The asymmetric unit contains one zinc atom, two vanadium atoms, two phosphorus atoms, eleven oxygen atoms, and one alkaline atom (Figure 3). Bond lengths are listed in Table 2. The vanadium atoms are bonded to oxygen atoms to form the classical distorted octahedron with four equatorial bonds ($\bar{d}_{V-O} \approx 2.02$ Å), a typical vanadyl V=O bond at $d \approx 1.60$ Å and a longer trans V···O bond at $d = 2.32$ Å. As usually found in oxovanadium chemistry, the oxygen atom of the vanadyl group is not shared with other polyhedra. The VO_6 octahedra are part of dimeric unit V_2O_9 through face-sharing involving two equatorial oxygen atoms and the oxygen from the longer V···O bond. As a result, short V−V bond distance $d_{V-V} \approx 3.06$ Å occurs within the dimer. The dimers are corner-connected to phosphate groups (six PO_4 and one H_2PO_4)

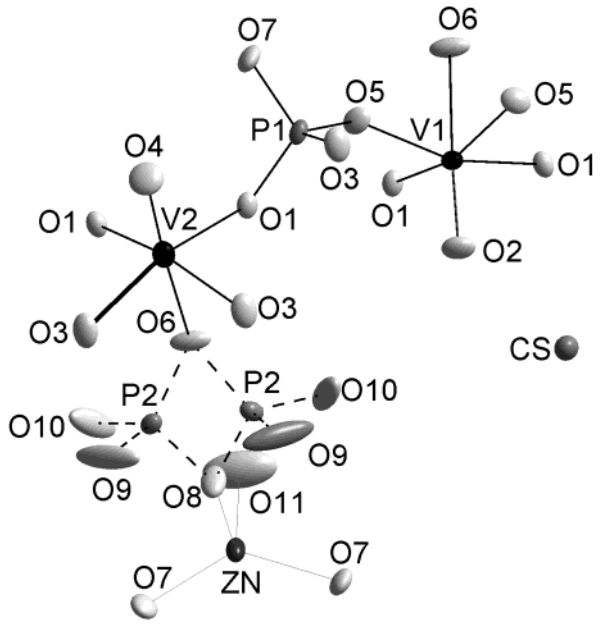

Figure 3. View of the asymmetric unit of $CsZn(H_2O)(VO)_2(PO_4)_2(H_2PO_4)$ (Ortep-style) showing the connectivity. Thermal ellipsoids are at the 65% probability level.

through di-μ-(O, O′)PO_4 (μ_2-links) and di-μ-(O)PO_4 bridges (μ_3-links). It is worth noting that the equatorial V−O bond strength is normally lowered with respect to the nature of the links at the shared oxygen atoms as the distances $d(V-(\mu_3-O))$ are longer than the corresponding $d(V-(\mu_2-O))$. Smaller V−O−P bond angles occur at the μ_3-links ($125.94(2)° \leq \alpha_{V-O-P} \leq 129.01(2)°$) in contrast to the bond angles at the μ_2-links ($145.23(2)° \leq \alpha_{V-O-P} \leq 146.66(2)°$). Though they are present as PO_4 and H_2PO_4 throughout the structure, the geometry of the phosphate groups is that usually observed for orthophosphates. The PO_4 make two μ_2- and one μ_3-oxo bridges with three dimers V_2O_9 and one μ_2-oxo bridge with the tetrahedron $ZnO_3(H_2O)$, whereas the H_2PO_4 groups make one μ_3-oxo bridge with one dimer V_2O_9 and one μ_2-oxo bridge with the tetrahedron $ZnO_3(H_2O)$, the latter two apexes being as terminal P−OH. Though the average P−O bond distances are almost equal, with values ranging from 1.53 Å (PO_4) to 1.54 Å (H_2PO_4), one can see that $d(P-O\mu_3) \approx d(P-OH) \gg d(P-O\mu_2)$ with the exception of the rubidium compound in which one observes surprisingly $d(P-O\mu_3) \ll d(P-OH)$. As usual, the slight lengthening observed for the H_2PO_4 group reflects the presence of terminal OH groups. Zinc tetrahedra ensure additional connectivity through the corner-sharing (μ_2-links) of three apexes with three phosphate groups, and the remaining free apex corresponds to the longer Zn−O bond distance to the water molecule. The P−O−Zn bond angles range from ca. 134° to 140°. The inhomogeneous near neighboring of the zinc atoms (two PO_4, one H_2PO_4, and one water molecule) results in significant distortions from the tetrahedral geometry. The Zn−O bond lengths range from 1.89 to 2.073 Å and the intra-polyhedral angles O−Zn−O vary between 100° and 132°. The so-obtained negatively charged 3D framework $[Zn(H_2O)(VO)_2(PO_4)_2(H_2PO_4)]^-$ generates tunnels of approximate section 6 × 3 Å^2 running along the [110] direction that are covered with OH and H_2O in which the alkaline cations occupy half their respective sites in a disordered manner (Figure

Table 2. Selected Bond Lengths (Å) with Their Standard Deviations for $CsZn(H_2O)(VO)_2(PO_4)_2(H_2PO_4)$, $KZn(H_2O)(VO)_2(PO_4)_2(H_2PO_4)$, and $RbZn(H_2O)(VO)_2(PO_4)_2(H_2PO_4)$

				$CsZn(H_2O)(VO)_2(PO_4)_2(H_2PO_4)$						
V1	-O1	1.586(3)	V2	-O7	1.584(3)	Zn	-O4	1.889(2)	Cs	-O1	2.924(2)
	-O2	1.964(2)		-O5	1.963(2)		-O4	1.889(2)		-O6	2.928(1)
	-O2	1.964(2)		-O5	1.963(2)		-O9	1.929(3)		-O8	2.993(5)
	-O3	2.067(2)		-O3	2.078(2)		-O10	2.099(4)		-O7	2.984(2)
	-O3	2.067(2)		-O3	2.078(2)		-O10	2.099(4)		-O10	3.050(5)
	-O6	2.321(3)		-O6	2.313(3)					-O9	3.191(2)
	-V2	3.063(1)		-V1	3.063(1)					-O2	3.247(2)
										-O5	3.359(2)
										-O10	3.413(4)
P1	-O5	1.521(2)	P2	-O9	1.491(3)						
	-O4	1.522(2)		-O11	1.556(5)						
	-O2	1.526(2)		-O6	1.598(3)						
	-O3	1.563(2)		-O8	1.537(4)						
				$KZn(H_2O)(VO)_2(PO_4)_2(H_2PO_4)$							
V1	-O1	1.588(2)	V2	-O7	1.591(2)	Zn	-O4	1.903(2)	K	-O8	2.464(3)
	-O2	1.969(1)		-O5	1.950(2)		-O4	1.903(2)		-O6	2.683(1)
	-O2	1.969(1)		-O5	1.950(2)		-O9	1.933(2)		-O1	2.757(2)
	-O3	2.055(1)		-O3	2.067(1)		-O10	2.066(3)		-O8	2.830(3)
	-O3	2.055(1)		-O3	2.067(1)		-O10	2.066(3)		-O7	2.893(2)
	-O6	2.367(2)		-O6	2.300(2)					-O2	2.903(2)
	-V2	3.057(1)		-V1	3.057(1)					-O3	3.069(2)
										-O5	3.171(2)
										-O9	3.251(2)
P1	-O5	1.510(2)	P2	-O9	1.475(2)						
	-O4	1.517(2)		-O11	1.560(3)						
	-O2	1.520(1)		-O6	1.564(2)						
	-O3	1.565(1)		-O8	1.578(3)						
				$RbZn(H_2O)(VO)_2(PO_4)_2(H_2PO_4)$							
V1	-O4	1.593(2)	V2	-O12	1.593(2)	Zn	-O3	1.885(2)			
	-O10	1.947(2)		-O5	1.956(2)		-O6	1.893(2)			
	-O1	1.987(2)		-O7	1.974(2)		-O11	1.913(2)			
	-O2	2.055(2)		-O9	2.068(2)		-O13	2.064(2)			
	-O9	2.067(2)		-O2	2.082(2)						
	-O8	2.327(2)		-O8	2.304(2)						
	-V2	3.062(1)		-V1	3.062(1)						
P1	-O10	1.521(2)	P2	-O5	1.513(2)	Rb1	-O4	2.842(2)	Rb2	-O8	2.765(3)
	-O7	1.527(2)		-O6	1.520(2)		-O12	2.917(2)		-O4	2.811(3)
	-O3	1.527(2)		-O1	1.534(2)		-O15	2.920(3)		-O12	2.870(3)
	-O2	1.563(2)		-O9	1.568(2)		-O8	2.925(2)		-O14′	2.946(20)
							-O10	3.107(2)		-O1	3.131(3)
							-O11	3.146(2)		-O13	3.157(4)
							-O5	3.231(2)		-O7	3.287(3)
							-O9	3.302(2)		-O2	3.324(3)
							-O13	3.393(3)		-O11	3.327(3)
P3	-O11	1.503(2)	P3′	-O11	1.504(4)						
	-O8	1.518(2)		-O8	1.540(6)						
	-O15	1.559(2)		-O14′	1.577(16)						
	-O14	1.571(2)		-O15′	1.622(17)						

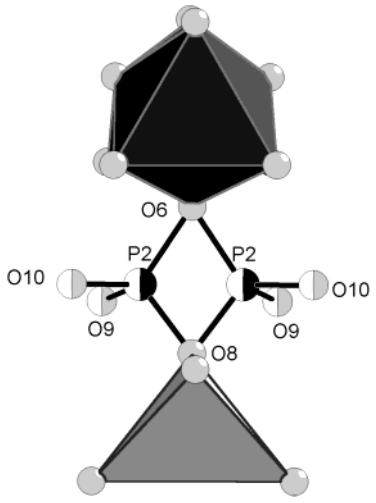

Figure 4. Illustration of the disorder for the H_2PO_4 groups.

4). At last, bond valence sum calculations[12] give formal oxidation states in good agreement with the expected values for V^{4+} (4.06(Rb) < Σs < 4.11(K)), P^{5+} (4.95 (Cs) < Σs < 5.01(Rb)), and Zn^{2+} (2.1 (K, Cs) < Σs < 2.2 (Rb)). The calculated lacks of ∼0.8 electrostatic valence units (e.v.u) for the free apexes around phosphorus and ∼1.6 e.v.u for the free apex around Zn indicate the presence of OH groups and a water molecule on the corresponding sites. The actual formula from the structure analysis $MZn(H_2O)(VO)_2(PO_4)_2(H_2PO_4)$ with the atomic ratios M/Zn/V/P = 1:1:2:3 agrees fairly well with the EPMA data for the heavy elements $K_{0.97(2)}Zn_{1.00(3)}V_{2.00(3)}P_{3.07(3)}$ (KZnVPO) and $Rb_{0.95}Zn_{1.06(4)}V_{2.00(3)}P_{3.00(3)}$ (RbZnVPO).

Discussion

The overall topology of $MZn(H_2O)(VO)_2(PO_4)_2(H_2PO_4)$ is very close to that of $(NH_4)Zn(H_2O)(VO)_2(PO_4)_2(H_2PO_4)$.[6] Close relationships also exist with the vanadyl hydrogen phosphate hemihydrate $VO(HPO_4)\cdot 0.5H_2O$[13]

(12) Brown, I. D.; Altermatt, D. *Acta Crystallogr.* **1985**, *B41*, 244.

that are discussed in detail in ref 3. The differences between the various structures are subtle and consist of local order/disorder mechanism involving the H_2PO_4 groups and the M^+ cations (Figure 4). The unit cells of (NH_4)ZnVPO and RbZnVPO (cell **1**) are twice those of CsZnVPO and KZnVPO (cell **2**) with the parameters related through $\mathbf{a}_1 = -\mathbf{a}_2 + \mathbf{c}_2$; $\mathbf{b}_1 = \mathbf{b}_2$; and $\mathbf{c}_1 = -(\mathbf{a}_2 + \mathbf{c}_2)$. Careful examination of the frames obtained from data collection for CsZnVPO and KZnVPO clearly shows the absence of diffraction spots which would lead to the supercell of (NH_4)ZnVPO. When looking after the space groups for (NH_4)ZnVPO and CsZnVPO, respectively $P2_1/n$ and $P2_1/m$, the translation $\mathbf{T}_1 = (\mathbf{a}_1 + \mathbf{c}_1)/2$ in cell **1** transforms as the fundamental translation vector $\mathbf{T}_2 = -\mathbf{a}_2$ in cell **2**, and as a consequence the possibility of removing the disorder is ruled out. Consequently, the random distribution for these compounds can be thought of as an intrinsic property of the structure. The so-observed disorder does not modify the overall topology of the different structures and it seems reasonable to consider that the synthetic pathways to obtain the different structures are energetically very close. According to the preceding, the X-ray powder patterns of KZnVPO and RbZnVPO were fully indexed in cell **2** as it provides the highest attainable figures of merit F_N and M_N. According to the formula $MZn(H_2O)(VO)_2(PO_4)_2(H_2PO_4)$, the measured density for KZnVPO ($\rho_{obs.} = 2.88$ g.cm^{-3}) compares fairly well with the calculated one ($\rho_{calc.} = 2.91$ g.cm^{-3}). The above formula is also very well supported by the thermal behavior of KZnVPO and RbZnVPO with losses of weight very close to those calculated (obs = 6.3%, calc = 6.6% for KZnVPO; obs = 5.9%, calc = 6.1% for RbZnVPO). Both compounds behave similarly and the dehydration reaction is complete at 800 K. To account for the experience, one can propose that $MZn(H_2O)(VO)_2(PO_4)_2(H_2PO_4) \rightarrow MZn(VO)_2(PO_4)_2(H_2PO_4) + H_2O$ occurs first, followed by water elimination through homocondensation of the phosphate species according to $MZn(VO)_2(PO_4)_2(H_2PO_4) \rightarrow MZn(VO)_2(PO_4)_2(PO_3) + H_2O$. The IR spectra sketched in Figure 1 support this mechanism as follows: (i) at 300 K the bands characteristic of orthophosphates species are clearly visible (P−O stretching ranging from 1150 cm^{-1} to 1000 cm^{-1}, P−O−H stretching in the range 2500 cm^{-1} to 3400 cm^{-1}) together with bands of the water molecule (O−H bending at ∼1640 cm^{-1}, O−H stretching at ∼3550 cm^{-1}); (ii) the O−H bending and stretching bands of the water molecule are not yet visible at 600 K; and, at last, (iii) at 850 K, the broad P−O−H stretching band of dihydrogenphosphate around 3200 cm^{-1} has disappeared, whereas the P−O−P stretching band characteristic of metaphosphate species is observed at ∼745 cm^{-1}.[14,15]

Magnetic Properties. All the compounds show an upturn on the susceptibility curve at $T < 12$ K that can be ascribed to small amounts of nonmagnetic V^{5+} ions or isolated V^{4+} centers. The calculated BVS for vanadium seemingly agrees fairly well with the presence of small amounts of V^{5+} ($4.06 \leq$ BVS $V^{x+} \leq 4.11$). If such, the compounds are nonstoichiometric as a deficit of hydrogen ions is needed to compensate the charge increase on the VPO framework, and the actual formula would be $MZn(H_2O)(V^{IV}_{(1-x)}V^{V}_{x}O)_2(PO_4)_2(H_{2-x}PO_4)$ with $x \sim 5\%$. However, supposing that the deviations of the BVS from the ideal value of 4 are not significant, the presence of isolated V^{4+} only reflects the finite size of the crystals in the bulk and the compounds are actually stoichiometric. Strikingly, all the compounds we are dealing with show the same amount of paramagnetic impurities (about 5%). Making the assumption that the peculiar ratio $V^{4+}/V^{5+} \approx 95{:}5$ is unlikely whatever the synthetic conditions, it seems reasonable to conclude that these compounds presented herein are in fact stoichiometric. On the basis of the structural results, the spin Hamiltonian for the Heisenberg alternating linear chain in zero field $\mathbf{H} = -J\sum_{i=1}^{n/2} (\hat{\mathbf{S}}_{2i}\cdot\hat{\mathbf{S}}_{2i-1} + \alpha\hat{\mathbf{S}}_{2i}\cdot\hat{\mathbf{S}}_{2i+1})$ was used to fit the data where J is the exchange integral and α is the alternation coefficient along the chain. At the extremes, **H** reduces to the HDVV Hamiltonian $\mathbf{H} = -J\hat{\mathbf{S}}_1\cdot\hat{\mathbf{S}}_2$ ($\alpha = 0$) for the dimer model with pairwise interactions and to $\mathbf{H} = -J\sum_{i=1}^{n-1} (\hat{\mathbf{S}}_i\cdot\hat{\mathbf{S}}_{i+1})$ ($\alpha = 1$) for the regular linear chain. The susceptibility data have been analyzed using three models: $\chi_{\mathbf{dm}} = (1-x)\chi_{\mathbf{d}} + x\cdot\chi_{\mathbf{i}}$ (dimer model **[1]**), $\chi_{\mathbf{acm}} = (1-x)\chi_{\mathbf{ac}} + x\cdot\chi_{\mathbf{i}}$ (alternating linear-chain model **[2]** with $\alpha > 0$), or simply $\chi_{\mathbf{acm}} = \chi_{\mathbf{ac}}$ (alternating linear-chain model **[3]** with $\alpha < 0$), where $\chi_{\mathbf{i}} = 3\,g^2/32T$ in the above formulas accounts for the paramagnetic behavior at low temperature and x is the amount of isolated V^{4+}. Whatever the model used to fit the data, the adjustable parameters were obtained from nonlinear regression analysis. The rounded maximum on the susceptibility curve at $T_{max} \approx 50$ K clearly indicates that the prevailing interactions are antiferromagnetic. The exchange parameter was roughly estimated $J \approx -55$ cm^{-1} from the experimental susceptibility curve considering the regular linear-chain model ($\alpha = 1$) as $kT_{max} \approx 1.282|J|$ at the susceptibility maximum.[16] The dimer model **[1]** $\chi_{\mathbf{dm}} = (1-x)\chi_{\mathbf{d}} + x\cdot\chi_{\mathbf{i}}$ with $\chi_{\mathbf{d}}$ equated according to Bleaney−Bowers[17] resulted in $g = 1.98(1)$, $J = -54.4(2)$ cm^{-1}, $x = 0.051(1)$ (KZnVPO); $g = 2.01(2)$, $J = -55.9(2)$ cm^{-1}, $x = 0.084(1)$ (RbZnVPO). Similar calculations were made using the analytical expression $\chi_{\mathbf{ac}} = Ng^2\beta^2(A + By + Cy^2)/(kT\cdot(1 + Dy + Ey^2 + Fy^3))$ for an alternating chain of local spins $^1/_2$ where the coefficients A, B, C, D, E, and F depend on the value of the alternation parameter α and $y = |J|/kT$. The use of model **[2]** resulted in $J = -54.8(4)$ cm^{-1}, $\alpha = 0.11(2)$, $g = 2.00(1)$, $x = 0.052(1)$ (KZnVPO) and $J = -55.8(9)$ cm^{-1}, $\alpha = 0.06(5)$, $g = 2.02(2)$, $x = 0.081(5)$ (RbZnVPO); while model **[3]** led to $J = -51.6(6)$ cm^{-1}, $\alpha = -0.082(4)$, $g = 1.94(2)$ (KZnVPO) and $J = -51(2)$ cm^{-1}, $\alpha = -0.14(2)$, $g = 1.97(5)$ (RbZnVPO). The best fits for the three models are shown in Figure 5. It is worthwhile noting that the spin distribution along the chain for model **[2]** is - -↑↓- -↑↓- -↑↓- -↑↓- - ($\alpha > 0$), whereas model **[3]** corresponds to - -↑↓- -↓↑- -↑↓- -↓↑- - ($\alpha < 0$). Moreover, paramagnetic impurities are not necessary to account for the experimental susceptibility data with model **[3]**.

(13) (a) Torardi, C. C.; Calabrese, J. C. *Inorg. Chem.* **1984**, *23*, 1308. (b) Leonowicz, M. E.; Johnson, J. W.; Brody, J. F.; Shannon, H.; Newsam, J. M. *J. Solid State Chem.* **1985**, *56*, 370.
(14) Rulemont, A.; Cahay, R.; Liegeois-Duyckaerts, M.; Tarte, P. *Eur. J. Solid State Inorg. Chem.* **1991**, *28*, 207.
(15) Corbridge, D. E. C.; Lowe, E. J. *J. Chem. Soc.* **1954**, 493.
(16) Bonner, J.; Fischer, M. *Phys. Rev.* **1964**, 135.
(17) Bleaney, D.; Bowers, K. D. *Proc. R. Soc. London* **1952**, *A214*, 451.

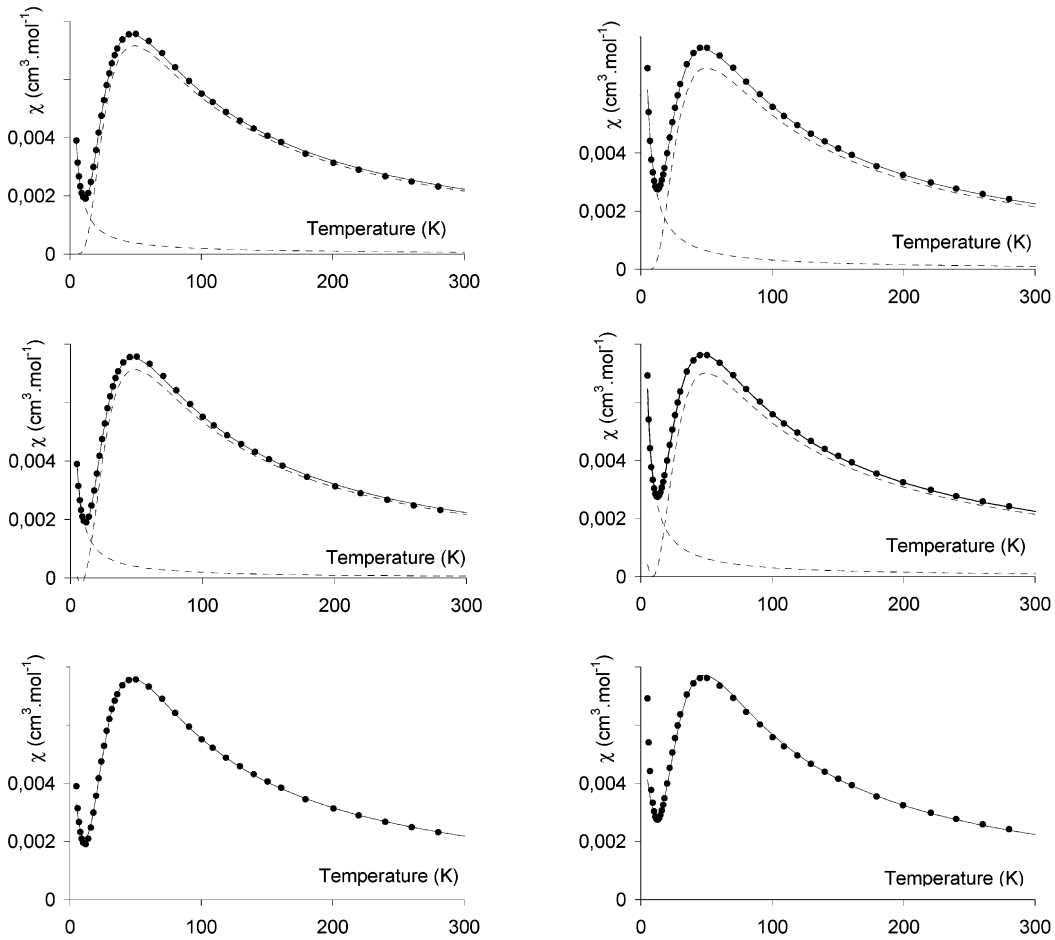

Figure 5. Fits of the $\chi = f(T)$ curves for KZnVPO (right) and RbZnVPO (left): black points, experimental; full line, best fit. From the top to the bottom: dimer model, alternating chain with $\alpha > 0$, and alternating chain with $\alpha < 0$ (see text).

Analysis of the preceding results leads to the following comments: (i) the nature and the magnitude of the exchange coupling and the *g* value are not sensitive to the model, and (ii) the amount of paramagnetic impurities and the spin distribution of the magnetic centers are strongly depending on the sign of the alternation parameter α. Obviously, all the three models satisfactorily fit the experimental data, and it is difficult to conclude what is the true nature of the couplings in these solids which is a well-known situation in the chemistry of oxovanadium phosphates.[18−20] As an example, several theoretical studies have been carried out to interpret the magnetic properties of the three different reported phases of the vanadyl pyrophosphate $(VO)_2P_2O_7$.[18,21−23] Relative magnitudes of spin exchange interactions were estimated on the basis of molecular calculations for the spin dimers. It has been shown that magnetic behavior for this compound and other oxovanadium phosphates can be correlated with the structural data focusing the topological features concerning the environment of the phosphate bridges entities. Most of these studies were carried out on the basis of extended Hückel calculations.[15,18,19] Because of the lack of ab initio estimations of exchange values, Robert et al. recently computed the magnetic exchange constants of $(VO)_2P_2O_7$ on the basis of a combined DFT/broken symmetry approach.[23] Such a study for MZnVPO's is in progress. Preliminary results indicate that the exchange interactions can be described in first approximation on the basis of the alternating antiferromagnetic chain model.[24]

Conclusion

The new solids MZnVPO with $M^+ = K^+$, Rb^+, and Cs^+ have been obtained. Their crystal structure is three-dimensional and the overall topology results from the heterocondensation of face-shared octahedra $[V_2O_9]$ with tetrahedra $[Zn(H_2O)O_3]$ and phosphate units $[H_2PO_4]$ and $[PO_4]$. The susceptibilities are indicative of low-dimensional magnetism with prevailing antiferromagnetic interactions. Surprisingly, the three models consistent with the structural features fit satisfactorily the susceptibility data, but do not allow elucidation of the actual magnetic pathways in these solids. Further studies involving theoretical studies using the DFT methods are in progress to determine the true nature of the couplings in these solids.

(18) Roca, M.; Amorós, P.; Cano, J.; Marcos, M. D.; Alamo, J.; Beltrán-Porter, A.; Beltrán-Porter, D. *Inorg. Chem.* **1998**, *37*, 3167.
(19) Johnson, J. W.; Johnston, D. C.; Jacobson, A. J.; Brody, J. F. *J. Am. Chem. Soc.* **1984**, *106*, 8123.
(20) Villeneuve, G.; Suh, K. S.; Amorós, P.; Casañ-Pastor, N.; Beltran-Porter, D. *Chem. Mater.* **1992**, *4*, 108.
(21) Koo, H.-J.; Whangbo, M.-H. *Inorg. Chem.* **2000**, *39*, 3599.
(22) Koo, H.-J.; Whangbo, M.-H.; VerNooy, P. D.; Torardi, C. C.; Marshall, W. J. *Inorg. Chem.* **2002**, *41*, 4664.
(23) Petit, S.; Borshch, S. A.; Robert, V. *J. Am. Chem. Soc.* **2002**, *124*, 1744.
(24) Messaoudi, S.; Le Fur, E.; Pivan, J.-Y.; Furet, E.; Gautier, R.; in preparation.

Acknowledgment. We are indebted to Dr. T. Roisnel for the single crystal intensity data collection on the Kappa CCD diffractometer (Centre de Diffractométrie, Université de Rennes 1), and J.C. Jegaden and S. Maron (CMEBA, Université de Rennes 1) and M. Bohn (IFREMER, Brest) for their assistance in EPMA studies.

Supporting Information Available: X-ray crystallographic file (CIF). This material is available free of charge via the Internet at http://pubs.acs.org.

CM031090K